Effect of pH on the Pore Forming Activity and Conformational Stability of Ostreolysin, a Lipid Raft-Binding Protein from the Edible Mushroom *Pleurotus ostreatus*[†,‡]

Sabina Berne,[§] Kristina Sepčić,[§] Gregor Anderluh,[§] Tom Turk,[§] Peter Maček,[§] and Nataša Poklar Ulrih*[,||]

Department of Biology, Biotechnical Faculty, University of Ljubljana, Veèna pot 111, 1000 Ljubljana, Slovenia, and Department of Food Science and Technology, Biotechnical Faculty, University of Ljubljana, Jamnikarjeva 101, 1000 Ljubljana, Slovenia

Received May 30, 2005; Revised Manuscript Received June 28, 2005

ABSTRACT: Ostreolysin, a pore-forming protein from the edible oyster mushroom (*Pleurotus ostreatus*), is a member of the aegerolysin protein family, a novel group of small acidic proteins found in bacteria, molds, mushrooms, and plants. It binds to lipid rafts and interacts specifically with cholesterol-rich lipid domains. In this study, ostreolysin was classified as a single-domain all-β-structured protein on the basis of cDNA sequencing. pH-induced and thermally induced unfolding of ostreolysin was studied by means of CD, UV absorption, and intrinsic tryptophan fluorescence to characterize conformational transitions associated with its functional properties, i.e., binding to lipid membranes, pore forming activity on lipid vesicles, and hemolysis. At 25 °C and between pH 6 and 9, ostreolysin adopted a monomeric and thermodynamically stable nativelike conformation, characterized by rigid tertiary structure and predominantly β-sheet secondary structure. Between pH 2 and 3, the protein underwent an irreversible transition to a partially unfolded, molten globule-like state which bound ANS, and exhibited disrupted tertiary structure and enhanced non-native α-helical structure. Functional studies showed that, unlike colicins and some other bacterial pore-forming toxins, the acid-induced molten globule-like state of ostreolysin is not relevant for lipid binding and pore formation. Instead, the compact native state was necessary for binding to cholesterol/sphingomyelin multilamellar vesicles, optimally in the pH range from 6 to 7, and for pore formation and hemolysis, maximally between pH 7 and 8.

Characterization of ostreolysin and aegerolysin (*1*, *2*), ∼15 kDa acidic proteins from the edible mushrooms *Pleurotus ostreatus* (oyster mushroom) and *Agrocybe aegerita* (black poplar mushroom), respectively, led to them being assigned to a novel aegerolysin protein family (PF06355 and IPR 009413). Other family members are Asp-hemolysin from the pathogenic mould *Aspergillus fumigatus* (*3*), pleurotolysin A (PlyA) from *P. ostreatus*, an ostreolysin isoform (*4*, *5*), two *Clostridium bifermentans* hemolysin-like proteins (*6*), a hypothetical protein PA0122 from *Pseudomonas aeruginosa* (*7*), a putative protein from *Neurospora crassa* (*8*), and proteins predicted from the expressed sequence tag (EST)[1] and genomic nucleotide sequences (Figure 1). Aegerolysin and ostreolysin are expressed specifically during the formation of primordia and fruiting bodies (*1*, *2*). Immunolocalization showed that they are concentrated in the growing regions of the basidiocarp, especially in basidia and spores (*9*). It has been proposed that aegerolysin is involved in the compaction of hyphae during the formation of fruiting body primordia (*2*), and that *C. bifermentans* hemolysin-like proteins are related to bacterial sporulation (*6*). However, the exact biological function of aegerolysins remains to be resolved.

Interaction with lipids and pore forming activity are characteristic of certain aegerolysins. Asp-hemolysin was suggested to bind specifically to lysophosphatidylcholine, a component of oxidized low-density lipoprotein (*3*, *10*, *11*). Aegerolysin, ostreolysin, and PlyA were reported to lyse erythrocytes and several transformed cell lines by creating transmembrane pores (*1*, *4*, *12*). Binding and pore forming activity of ostreolysin, inhibited by the presence of unsaturated glycerophosphatides and lysophospholipids (*12*, *13*), were found to be specific to liquid-ordered microdomains, structures emerging in cholesterol- and ergosterol-rich lipid membranes, and lipid rafts (*13*). PlyA has been suggested to be a sphingomyelin-specific cytolysin, acting as a bicomponent cytolysin in concert with 59 kDa pleurotolysin B (PlyB). On erythrocyte membranes, PlyA and PlyB (when

[†] This work was supported by the Ministry of Higher Education, Science and Technology of the Republic of Slovenia.

[‡] GenBank entry AY818435 (*P. ostreatus* ostreolysin mRNA, partial coordinates).

* To whom correspondence should be addressed. Telephone: +386 1 423 11 61. Fax: +386 1 256 62 98. E-mail: natasa.poklar@bf.uni-lj.si.

[§] Department of Biology.

[||] Department of Food Science and Technology.

[1] Abbreviations: ANS, 8-anilinonaphthalene-1-sulfonic acid; CD, circular dichroism; Chol, cholesterol; DTT, dithiothreitol; EST, expressed sequence tag; GnHCl, guanidine hydrochloride; $\Delta C_p°$, apparent standard heat capacity difference between the denatured and native state of ostreolysin; $\Delta G°_d(T)$, Gibbs free energy; $\Delta H°_d(T)$, denaturation enthalpy; $\Delta S°_d(T)$, denaturation entropy; $\Delta H°_{vH}$, van't Hoff enthalpy of denaturation; HEPES, 4-(2-hydroxyethyl)-1-piperazineethanesulfonic acid, monosodium salt; LUV, large unilamellar vesicles; MES, 2-morpholinoethanesulfonic acid; MLV, multilamellar vesicles; MW, molecular weight; SEL, sheep erythrocyte lipids; SM, sphingomyelin; T_d, temperature at the denaturation midpoint.

10.1021/bi051013y CCC: $30.25
Published on Web 07/30/2005

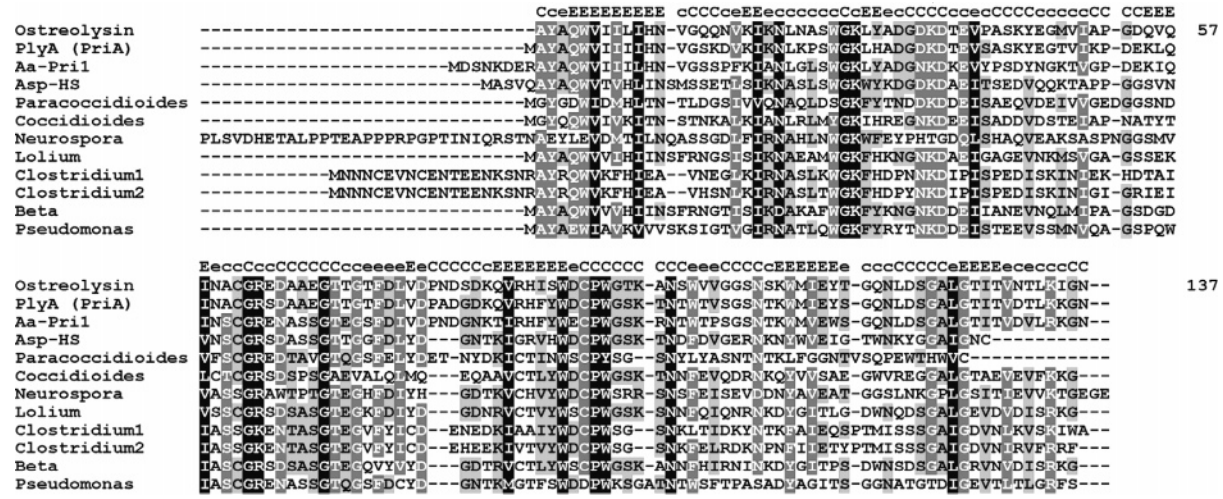

FIGURE 1: Sequence alignment of the aegerolysin family. The family comprises ostreolysin (GenBank entry AY818435) and 11 other members. Protein and nucleotide databases were searched with BLAST using the ostreolysin sequence as a query. Hits with *e* values of less than $2e^{-9}$ are presented. Strictly conserved residues are shown in black and similar residues in gray. The numbering is according to the ostreolysin sequence. The PHD secondary structure prediction (*25*, *26*) is shown above the alignment (E, extended strand; C, random coil). Uppercase letters are predicted at better than 82%. Proteins are abbreviated as follows: PriA, putative protein from *P. ostreatus* (GenBank entry AAL57035), identical to PlyA, protein from *P. ostreatus* (DDBJ, GenBank entry AB177869); Aa-Pri1, aegerolysin precursor (Swiss-Prot entry O42717); Asp-HS, Asp-hemolysin precursor (GenBank entry Q00050); Paracoccidioides and Coccidioides, predicted proteins from pathogenic fungi *Pa. brasiliensis* (GenBank entry CN242319) and *C. immitis* (cid07143); Neurospora, hypothetical protein from *N. crassa* (GenBank entry XP_322733); Lolium, predicted protein from *Lolium multiflorum* (GenBank entry AU250367); Clostridium 1 and 2, hemolysin-like proteins from *C. bifermenta*s (GenBank entries CAA71483 and CAA71484, respectively); Beta, predicted protein from *B. vulgaris* (GenBank entry BQ583143); Pseudomonas, conserved hypothetical protein from *Ps. aeruginosa* (GenBank entry NP_248812).

coupled, termed pleurotolysin) assemble into a ring-shaped transmembrane pore with a functional diameter ranging from 3.8 to 5.0 nm (*4*, *5*). In contrast, ostreolysin alone was found to form pores ~4 nm in diameter (*12*).

Certain cell proteins need to be actively unfolded from their native conformation to be translocated across membranes into a specific compartment by translocons or to be degraded by ATP-dependent proteases (*14*). On the other hand, pore-forming proteins (toxins, complement proteins, and pro-apoptotic proteins) are examples of proteins with a defined native conformation, which, upon an environmental trigger, is changed spontaneously to enable formation of a transmembrane pore consisting of several protein monomers (*15*). Although high-resolution three-dimensional structures of such pores are lacking, there is indirect evidence that these proteins undergo several structural changes during membrane binding, oligomerization, insertion, and translocation of certain polypeptide segments across the lipid bilayer (*15*, *16*) to reach a thermodynamically more favorable membrane-resident protein conformation. In our previous study, we noted that ostreolysin permeabilization of lipid vesicles was pH-dependent, with the highest activity around pH 8. Moreover, FTIR spectroscopy showed that ostreolysin is a predominantly β-structured protein whose content of α-structure increased by ~10% on association with the vesicles (*12*).

Here, we address the question of how conformational changes of ostreolysin are related to pH and temperature, and whether the induced protein unfolding is relevant to its pore forming activity in cells and artificial lipid membranes.

MATERIALS AND METHODS

Materials

Ostreolysin was isolated from fresh fruiting bodies of *P. ostreatus*, as described previously (*1*). Its purity was checked by polyacrylamide gel electrophoresis. The protein concentration was determined spectrophotometrically using the BCA Protein Assay Reagent (Pierce, Rockford, IL).

Total sheep erythrocyte lipids (SEL) were extracted from pelleted erythrocyte ghosts as described previously (*12*). Extracted lipids were dried under argon and dissolved in chloroform at a concentration of 10 mg/mL. Wool grease cholesterol (Chol) and porcine brain sphingomyelin (SM) were from Avanti Polar Lipids (Alabaster, AL).

ANS (1-anilinonaphthalene-8-sulfonic acid ammonium salt) and guanidine hydrochloride (GnHCl) were from Fluka (Buchs, Switzerland). ANS was used without additional purification. GnHCl was recrystallized from hot ethanol, and a 5.0 M solution (pH 5.0) was prepared in doubly distilled water. Dithiothreitol (DTT), oxidized glutathione, Triton X-100, 2-morpholinoethanesulfonic acid (MES), and calcein were from Sigma. NaOH and HCl used in the pH titration experiments were from Merck (Darmstadt, Germany).

For the thermal stability studies, the following 10 mM buffers were used: citrate (pH 3.0), carbonate (pH 6.0, 10.0, and 11.0), HEPES (pH 7.0 and 8.0), and borate (pH 9.0). For assaying the pore forming activity of ostreolysin and its binding to lipids in the pH range from 7.0 to 9.0, vesicle buffer (140 mM NaCl, 20 mM Tris-HCl, and 1 mM EDTA) was used; for pH values ranging from 4.0 to 6.0, MES was used instead to prepare the buffer. All chemicals were analytical grade.

Methods

Cloning of Ostreolysin cDNA. Freshly collected young (1.5 cm) fruiting bodies of the oyster mushroom were ground under liquid nitrogen to a medium-fine powder. Total cellular RNA was extracted from 30 mg of ground tissue by using the SV Total RNA Isolation System (Promega, Madison,

WI). 3′ RACE was performed essentially as described in the FirstChoice RLM-RACE kit (Ambion). RT-PCR was conducted with the 3′ RACE Adapter (5′-GCGAGCACAGAATTAATACGACTCACTATAGGT$_{12}$VN-3′) and M-MLV Reverse Transcriptase, using 1 μg of total RNA. The ostreolysin cDNA was produced in a PCR using 1 μL of RT-PCR mixture, 3′ RACE inner primer (5′-CGCGGATCCGAATTAATACGACTCACTATAGGT$_{12}$VN-3′), AYAQWV-BAM gene-specific primer (5′-CGCGGATCCGCNTAYGCNCARTGGGTNAT-3′), Vent$_R$ (exo−) DNA polymerase (New England BioLabs Inc.), and ThermoPol reaction buffer (New England BioLabs Inc.). An AYAQWV-BAM coding oligonucleotide was designed according to the six conserved N-terminal amino acids of proteins of the aegerolysin family. Both the 3′ RACE inner primer and AYAQWV-BAM gene-specific primer contained a *Bam*HI site to enable cloning after amplification. The PCR mixtures were heated at 94 °C for 3 min (hot start), and amplification was then carried out in 25 cycles as follows: denaturation for 1 min at 94 °C, annealing for 45 s at 60 °C, and extension for 1 min at 72 °C. A final extension was conducted for 10 min at 72 °C. The resulting PCR products were gel purified using a Qiaquick extraction kit (Qiagen), digested with *Bam*HI (New England BioLabs Inc.), and ligated into pUC19. The nucleotide sequence of ostreolysin cDNA was determined in both directions and the amino acid sequence deposited in GenBank under accession number AY818435.

pH Measurements. The pH titration experiments at 25 °C were performed using a 10 μL Hamilton syringe (Hamilton Co., Reno, NV) equipped with a Chaney adapter. The pH of protein solutions was measured separately using a pH-meter (model MA 5705, Iskra) and an Ag/AgCl combination microelectrode (Mettler Toledo). The absolute error of the pH measurements was ±0.01 pH unit.

Electrophoresis. SDS−PAGE was performed with a PHAST system (Amersham Pharmacia Biotech, Uppsala, Sweden) according to the manufacturer's instructions (*17*), using PhastGel Gradient 8−25 gels at 25 °C. The protein samples were diluted with an equal volume of the nonreducing SDS sample buffer [0.20 M Tris-HCl (pH 8.0), 5% (w/v) SDS, 2 mM EDTA, and 0.1% (w/v) bromophenol blue], heated at 100 °C for 5 min, and applied to the gel. Gels were stained with Coomassie Brilliant Blue or silver-stained. Images were documented and processed using Image-Pro Plus software (Media Cybernetics).

In some experiments, ostreolysin was treated with DTT (20 mM) for 30 min or with oxidized glutathione (10 mM) overnight, all at room temperature. Oxidized protein samples were submitted to SDS−PAGE. Hemolytic activity and binding of oxidized glutathione-treated ostreolysin to Chol/SM multilamellar vesicles were assessed as described below.

Pore Forming Activity. The pore forming activity of ostreolysin was assayed by determining the hemolytic activity and by calcein release from large unilamellar vesicles (LUV) composed of sheep erythrocyte lipids (SEL). The hemolytic activity of ostreolysin toward sheep, bovine, and human erythrocytes was closely similar (*12*). In this study, the hemolytic activity on bovine red blood cells (BRBC) was measured turbidimetrically (*18*) at 25 °C using a kinetic microplate reader (MRX, Dynex Technologies, Denkendorf, Germany). Typically, 25 μL of ostreolysin (4 μg/mL) was added to 75 μL of BRBC buffer (140 mM NaCl and 20 mM Tris-HCl buffer, with a pH ranging from 6.0 to 10.0) and the mixture incubated at room temperature for 30 min; 100 μL of bovine erythrocyte suspension at the same pH as the ostreolysin solution was then added. The initial optical density of the solution at 630 nm (OD_{630}) was 0.5. The decrease in OD_{630} was recorded for 20 min to determine the time necessary for 50% hemolysis ($t_{0.5}$). In control experiments without ostreolysin, spontaneous lysis of the erythrocyte suspension was observed at pH values below 6 and above 10.

The effect of pH on permeabilization of SEL LUV by ostreolysin was measured as described previously (*12*). At a final concentration of 4 mg/mL, lipids were swollen in an aqueous solution of calcein (80 mM), and vortexed to obtain multilamellar vesicles (MLV). The suspension of MLV was subjected to eight cycles of freezing and thawing, and pressure-extruded through 0.1 μm polycarbonate filters (Millipore). Extravesicular calcein was removed by gel filtration on a Sephadex G-50 (medium) column. Vesicle permeabilization was assayed in a fluorescence microplate reader (Tecan Genios) with excitation and emission at 485 and 535 nm, respectively. Ostreolysin at the desired concentration in MES or Tris-HCl vesicle buffer (100 μL) was dispensed into a multiwell microplate, followed by an appropriate amount of calcein-loaded LUV. The rate of release of calcein was then recorded for 45 min at 25 °C. The maximal (100%) rate of calcein release was obtained by solubilization of LUV with Triton X-100 at a final concentration of 1 mM, and the percentage of calcein release was calculated for each well (*19*).

Ostreolysin Binding to Lipids. The effect of pH on the binding of ostreolysin to multilamellar lipid vesicles (MLV) was determined semiquantitatively by using SDS−PAGE of lipid-bound and free ostreolysin, and densitometry of silver-stained gels. MLV were prepared from Chol and SM (1:1 molar ratio) after evaporation of the solvent under reduced pressure and vortexing the lipid film in water to obtain a lipid concentration of 20 mg/mL. Aliquoted MLV suspensions were titrated using 1 M HCl or NaOH to adjust the pH to the desired value. Ostreolysin (1.2 mg/mL in water) was then added to obtain a lipid:protein molar ratio of 450, and the pH was checked. After incubation for 8 h at 25 °C, the mixture was centrifuged at 29000*g* for 30 min at room temperature. After removal of the supernatant containing unbound ostreolysin, the MLV were resuspended in MES or Tris-HCl vesicle buffer having the same volume as the supernatant. The fractions containing free or bound ostreolysin were subjected to SDS−PAGE and semiquantification of the protein using gel densitometry. In parallel, ostreolysin treated with oxidized glutathione was assayed for lipid binding. Control experiments without MLV showed no sedimentation of ostreolysin in the tested pH range.

Denaturation Studies. pH- and temperature-induced denaturation of ostreolysin were monitored using UV absorbance, circular dichroism (CD), and fluorescence.

UV Spectrophotometry. The UV absorbance was measured with a Hewlett-Packard 8453 UV−vis spectrophotometer (Hewlett-Packard GmbH, Waldbronn, Germany) equipped with an electro-thermal temperature controller, using a 1 cm path length quartz cuvette. Absorbance versus temperature profiles of ostreolysin (0.4−0.6 mg/mL) were obtained at 245 and 280 nm in the temperature range from 20 to 95 °C.

The temperature was increased in 1 °C increments, and protein samples were allowed to equilibrate for 1 min at each temperature.

Circular Dichroism Spectroscopy. Ellipticity was measured using an AVIV model 62A DS spectropolarimeter (AVIV Associates, Lakewood, NJ) equipped with a thermoelectrically controlled cell holder. Cuvettes with path lengths of 1 mm were employed for far-UV (200−260 nm) and 10 mm for near-UV (240−310 nm) measurements, with ostreolysin concentrations of 1 and 1.5 mg/mL, respectively. CD spectra were recorded as a function of temperature between 20 and 95 °C with a 5 °C step and as a function of pH at 25 °C. Spectra were corrected for solvent dichroism. The mean residue ellipticity, $[\Theta]_\lambda$, was calculated by using the relation

$$[\Theta]_\lambda = \frac{M_o \Theta_\lambda}{100cl} \quad (1)$$

where M_o is the mean residue molar mass (109.5 g/mol for ostreolysin), Θ_λ is the measured ellipticity in degrees, c is the concentration in grams per milliliter, and l is the path length in decimeters. $[\Theta]_\lambda$ was expressed in degrees square centimeter per decimole.

Secondary structure content was calculated from the far-UV CD spectra using the CONTIN software package (*20*).

Fluorescence Measurements. Fluorescence spectra were recorded with a Jasco FP-750 spectrofluorometer (Jasco Ltd., Essex, U.K.) equipped with a water-thermostated cell holder using a 1 cm path length quartz cuvette. Slit widths with a nominal band-pass of 5 nm were used for both excitation and emission. Intrinsic fluorescence emission spectra of ostreolysin were recorded from 300 to 500 nm as a function of pH. An excitation wavelength of 293 nm was used to follow tryptophan fluorescence. The emission spectra of ostreolysin, corrected for the solvent blank, were normalized for dilution and corrected for PM-tube response. The wavelengths at maximum emission intensity, λ_{max}, and the fluorescence intensity at 330 nm were determined.

ANS fluorescence was excited at 365 nm, and emission spectra were recorded from 400 to 600 nm as a function of temperature between 5 and 90 °C with a step of 5 °C, and as a function of pH between 1 and 13.

The steady-state intrinsic fluorescence of ostreolysin, either alone or combined with sheep erythrocyte LUV (in a 3.25 w/w ratio in MES or Tris-HCl vesicle buffer), was measured at 25 °C. Excitation and emission slits were set at 5 nm. Samples were excited at 295 nm. Fluorescence emission spectra of ostreolysin (320 nM) were recorded and corrected for the dilution factor, and the background was subtracted using appropriate blanks.

RESULTS

cDNA for ostreolysin was sequenced and shown to encode a 137-amino acid protein (calculated $M_r = 14\,854$, pI = 4.8) that belongs to the aegerolysin family (Figure 1). It contains 13 positively (Arg, Lys, and His) and 16 negatively (Asp and Glu) charged residues, a relatively high content of aromatic residues (six Trp, four Tyr, and two Phe residues), and two cysteine residues. Protein and nucleotide databases were searched with the ostreolysin amino acid sequence as a query, and 11 proteins with *e* values of less than $2e^{-9}$ were retrieved (Figure 1). Besides proteins belonging to the aegerolysin family, additional putative proteins or protein modules were obtained as translated from EST clones or predicted from genomic sequences (from *Ps. aeruginosa*, *Paracoccidioides brasiliensis*, *Coccidioides immitis*, *N. crassa*, *Lolium multiflorum*, and *Beta vulgaris*). The cDNA-derived primary structure of ostreolysin is 79% identical with ostreolysin isoform PlyA (*5*), and 62% identical with the aegerolysin sequence derived from the *Aa-Pri1* gene (*2*). The least similar member (protein from *N. crassa*) is 27% identical and 40% similar to ostreolysin. The cysteines, 61 and 93 in ostreolysin, and tryptophan residues (5, 27, 91, 95, 102, and 111) are conserved, implying their possible structural and/or functional roles. Intact cysteine residues have been reported to be indispensable for the hemolytic activity of ostreolysin (*1*) and Asp-hemolysin (*21*). The region of residues 91−102 contains three tryptophans and Cys93. Tryptophan-rich regions have been reported in some other pore-forming proteins and shown to be responsible for the initial attachment to the membrane (*22*, *23*). Combined aromatic residues and a cysteine residue have been suggested to be involved in sterol binding of cholesterol-dependent bacterial pore-forming toxins (*24*).

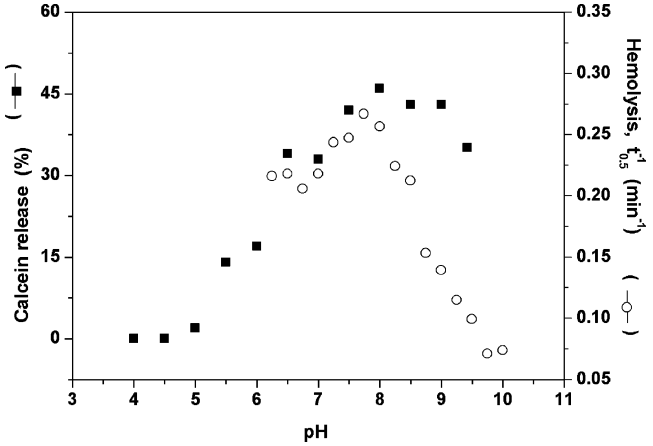

FIGURE 2: pH dependence of ostreolysin hemolytic activity and permeabilization of SEL LUV. The rate of hemolysis of bovine red blood cells (○), $1/t_{0.5}$, and the percentage of calcein release (■) were determined at 25 °C using 30 and 18 nM ostreolysin, respectively, as described in Materials and Methods.

Analysis of the secondary structure preferences of the ostreolysin polypeptide chain by the neural networks method PHD (*25*, *26*) gave 40% extended β-strand and 60% aperiodic secondary structure. The secondary structure prediction algorithms that were tested reported zero or less than 10% α-helix. Moreover, using 3D-PSSM (*27*), members of the aegerolysin family were predicted to be all-β proteins, and ostreolysin exhibited some structural resemblance to the lectin domain CATH Domain 1jlxA1.

Pore Forming Activity and Binding to Lipids. The dependence on pH of ostreolysin pore forming activity was studied on red blood cells and on lipid vesicles made of erythrocyte lipids. Figure 2 shows hemolytic activity compared with the rate of calcein release from SEL LUV. Below pH 6, spontaneous hemolysis was observed. Maximum hemolytic activity was observed at pH 7.8, while the rate of calcein release was maximal at pH 8.0.

Preincubation of ostreolysin with Chol/SM (1:1) LUV inhibited its hemolytic activity most efficiently at pH ∼6.0 (not shown). We therefore studied binding of ostreolysin to

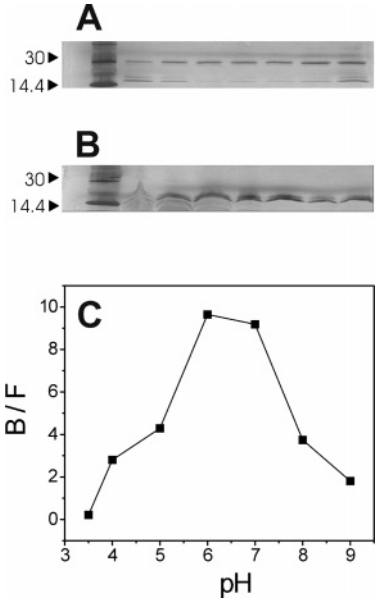

FIGURE 3: pH dependence of ostreolysin binding to Chol/SM multilamellar vesicles. Ostreolysin was incubated with Chol/SM (1:1 molar ratio) MLV at a lipid:protein molar ratio of 450 at the indicated pH, and centrifuged. Free ostreolysin (A) and ostreolysin bound to the pelleted MLV (B) were analyzed with SDS−PAGE; triangles indicate the molecular mass standards in kilodaltons. Densitometry was used to determine semiquantitatively the ratio of bound to free protein (B:F) in panel C.

the vesicles as a function of pH in more detail. After incubation with Chol/SM (1:1) MLV, fractions of free (Figure 3A) and lipid-bound (Figure 3B) ostreolysin were analyzed by SDS−PAGE and densitometry. Binding was maximal at pH 6−7 (Figure 3C). Increasing the pH induces formation of an ostreolysin dimer that is not capable of binding to the vesicles (Figure 3A).

It has been suggested that the microheterogeneity seen in SDS−PAGE may be ascribed to formation of an intramolecular disulfide bond between the two cysteine residues (*1*). If so, it could alter the protein conformational stability and consequently modify its biological activity. To eliminate this possibility, we treated ostreolysin with oxidized glutathione and with DTT. Neither of them affected the hemolytic activity of ostreolysin, suggesting that the disulfide bonds are not crucial for it.

Far-UV CD Spectra of Ostreolysin. In the pH range from 3.6 to 6, significant protein precipitation occurred. This was most probably due to isoelectric precipitation rather than conformational changes since (i) even at pH 7 and 8 ostreolysin solubility has been found to be rather low (up to ~2 mg/mL or ~130 μM) and (ii) the near-UV CD spectrum of ostreolysin at pH 3.5 was similar to those recorded at pH >6.

Representative far-UV and near-UV CD spectra of ostreolysin are compared to those recorded in 5 M GnHCl (Figure 4). A spectrum at pH 7.8 (Figure 4A) is characterized by a negative CD band near 218 nm, which is typical of β-structure (*28*). On the basis of CONTIN analysis, ostreolysin in aqueous solution at pH 7.8 contains 10 ± 3% α-helix, 60 ± 8% β-sheet, 6 ± 3% β-turn, and 24 ± 10% aperiodic secondary structure. These values agree reasonably with those predicted and obtained from FTIR spectroscopy (*12*).

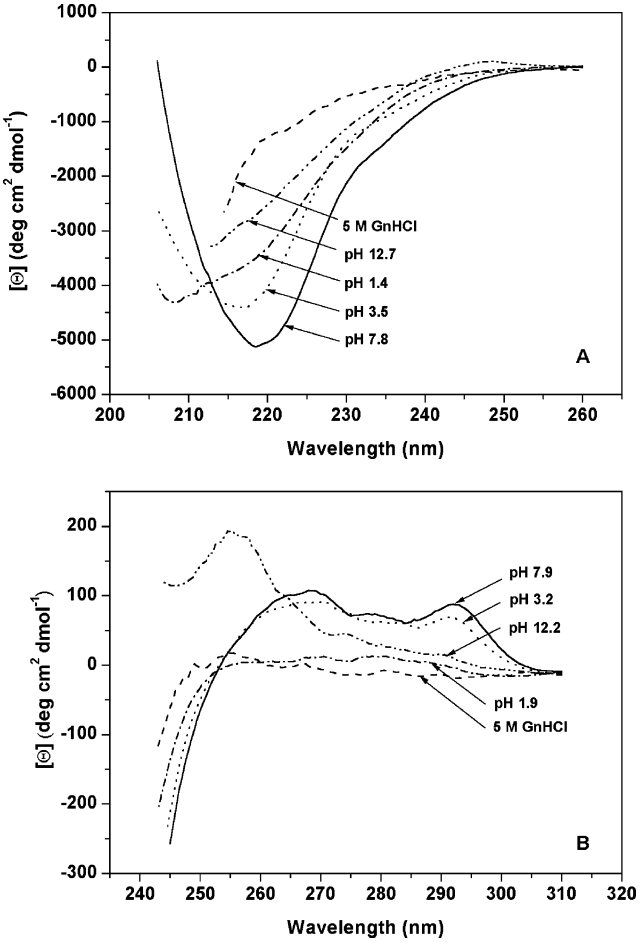

FIGURE 4: Dependence of CD spectra of ostreolysin on pH. Far-UV CD spectra of 66.7 μM ostreolysin (A) and near-UV CD spectra of 100 μM ostreolysin (B) were recorded at representative pH values at 25 °C. Guanidinium chloride (5 M GnHCl) was used to unfold the protein.

Reducing the pH from 7.8 to 1.1 caused a decrease in ellipticity, and two isodichroic points were observed at 208 and 210 nm (not shown), suggesting the existence of three spectroscopically different states of the protein. At low pH, there was a slight increase in the level of α-structure. For example, at pH 1.1, ostreolysin had 14 ± 1% α-helical structure, 49 ± 4% β-structure, and 37 ± 3% aperiodic secondary structure.

Increasing the pH from 7.8 to 13.0 was accompanied by an alteration of the shape and intensity of the far-UV CD spectrum, typical of a base-induced conformational transition. The spectra were blue-shifted, and the amount of aperiodic structure increased at the expense of β-structure. For example, at pH 12.1, ostreolysin had 7 ± 1% α-helix, 48 ± 3% β-structure, and 45 ± 3% aperiodic structure. Three isodichroic points were observed in the alkaline pH range (not shown), implying the presence of four different spectroscopic states of ostreolysin, probably due to deprotonation equilibria of basic amino acid side chains accompanied by conformational transitions. The spectrum at pH 12.7 resembled that of the unfolded polypeptide chain in 5 M GnHCl.

Near-UV CD Spectra of Ostreolysin. These spectra (Figure 4B), dominated by tryptophans and tyrosines, did not change significantly in the pH range from 3.2 to 9.2, as observed in far-UV CD spectra, suggesting stable tertiary and secondary

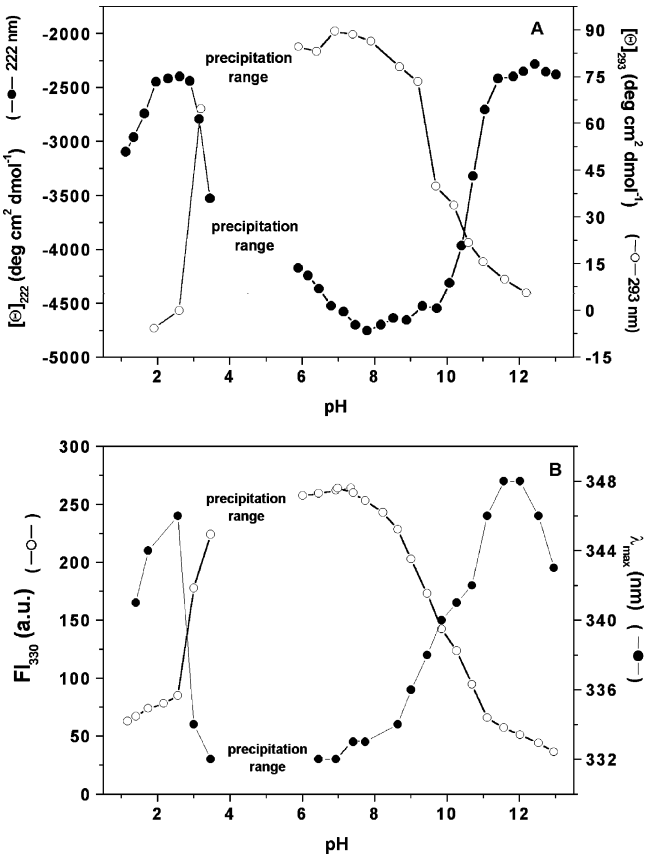

FIGURE 5: Dependence of ostreolysin structure on pH. CD (A) and fluorescence spectra (B) of 66.7 and 16.7 μM ostreolysin, respectively, were recorded at indicated pH values and 25 °C as described in Materials and Methods. (A) Changes in molar ellipticity at 222 (●) and 293 nm (○), indicating changes in secondary and tertiary structure, are presented. (B) Changes in the intensity of ostreolysin tryptophan fluorescence at 330 nm (○) and maxima of emission spectra, λ_{max} (●), at indicated pH values. Significant ostreolysin precipitation is denoted in the pH range of 3.5−6.5.

structure of ostreolysin. In the same pH range, two strong bands appeared, with maxima at 293 and 268 nm, together with a relatively weak band between 275 and 285 nm. At pH <2.6, the spectra closely resembled those for unfolded ostreolysin obtained in the presence of 5 M GnHCl, indicating the lack of defined tertiary structure. At pH >9.2, the intensity of the peak at 293 nm decreased, reflecting a reduced tryptophan contribution, probably due to increased protein dynamics. At pH >11.0, only one peak with a maximum at 245 nm appeared (Figure 4B), which can be ascribed to an ionized form of exposed tyrosine residues (*29*).

CD and Fluorescence Titration of Ostreolysin. Titration curves, derived from single spectra recorded at indicated pH values, are presented in Figure 5A. Changes in molar ellipticity followed at 222 nm in the pH range from 8 to 10 (Figure 5A) are not significant. The corresponding contents of secondary structure differed only moderately from those at pH 7.8 (for example, at pH 10, ostreolysin still retained 9% α-helical structure, 57% β-structure, and 34% aperiodic structure). In contrast, the changes in molar ellipticity followed at 293 nm over the same pH range are marked. These changes in the tertiary structure coincide with the deprotonation−protonation equilibria of two Cys residues (pK_a = 8.2), the $-NH_3^+$ terminus of the Ala residue (pK_a = 9.7), four Tyr residues (pK_a = 10.1), and nine Lys residues (pK_a = 10.5); the pK_a values in parentheses refer to the free amino acids. A further increase in pH from 10 to 12 caused sharp changes in molar ellipticity at 222 and 293 nm, as a consequence of disruption of the secondary and tertiary structure. The loss of most of the secondary structure and the complete loss of tertiary structure at pH >12 are most probably due to the deprotonation of four Tyr (pK_a = 10.1), nine Lys (pK_a = 10.5), and two Arg (pK_a = 12.5) residues.

It is expected that acid titration results in protonation of two His (pK_a = 6.0), five Glu (pK_a = 4.3), and 11 Asp (pK_a = 3.7) residues. The decrease in pH from 7.8 to 6.0 was accompanied by a reduction in the molar ellipticity at 222 nm but no change at 293 nm (Figure 5A). At pH 3.2, the near-UV CD spectrum can almost be superimposed on the one obtained at pH 7.8 (Figure 4B), indicating that ostreolysin still has a large portion of native tertiary structure. However, in the vicinity of the protein pI value, CD absorption data may be uncertain due to the protein−protein associations prior to precipitation, and the resulting flattening of spectra (*30*).

In the pH range from 2 to 3, ostreolysin contains a high level of secondary structure (17% α-helix, 45% β-structure, and 38% aperiodic structure) but no persistent tertiary interactions (Figure 4A,B). At pH <2.0, the proportion of aperiodic structure gradually increased; however, even at pH 1.1, ostreolysin still retained some secondary structure, unlike in 5 M GnHCl (Figure 4A).

Fluorescence emission spectra of ostreolysin in aqueous solution (data not shown) were typical of those generally observed for Trp-containing proteins (*31*). The fluorescence emission intensity followed at 330 nm in the alkaline pH range shows two transitions at pH 9 and 10.5 (pH of the transition midpoint), and one in the acid pH range at pH 3 (Figure 5B), which is in good agreement with the CD data (Figure 5A). Significantly different results can be observed by following the changes in the position of λ_{max}. In the pH range from 6 to 7, λ_{max} is practically constant (332 ± 1 nm). A slight red shift of 2 nm was observed in the pH range from 7 to 8, while a remarkable red shift, from 334 ± 1 to 348 nm, was observed in the pH range from 8 to 12. The fluorescence intensity decrease and red shifting suggest that the Trp indolyl nuclei are becoming exposed to the aqueous environment and ostreolysin adopts a fully denatured state. However, a further increase in pH above 12 caused a blue shift to 343 nm, suggesting partial rearrangement of the polypeptide chain into a conformational state, with certain Trp residues in a more hydrophobic environment. To summarize, the observed changes in the position of λ_{max} in the alkaline pH range suggest the existence of four pH-dependent spectroscopically distinguished states of ostreolysin.

A steep red shift of λ_{max} from 332 ± 1 to 347 ± 1 nm is observed by lowering the pH from 3.5 to 2.5, followed by a blue shift to 342 ± 1 nm at pH 1.5 (Figure 5B), suggesting two conformational transitions. The observed blue shift in the position of λ_{max} at pH <2.5, in combination with the far-UV CD data, reflects an increase in the amount of secondary structure, and suggests that the polypeptide chain is locally organized, with Trp residues buried in more hydrophobic environments. This is typical for formation of a molten globule-like state. Such a thermodynamically stable intermediate conformation is characterized by the presence

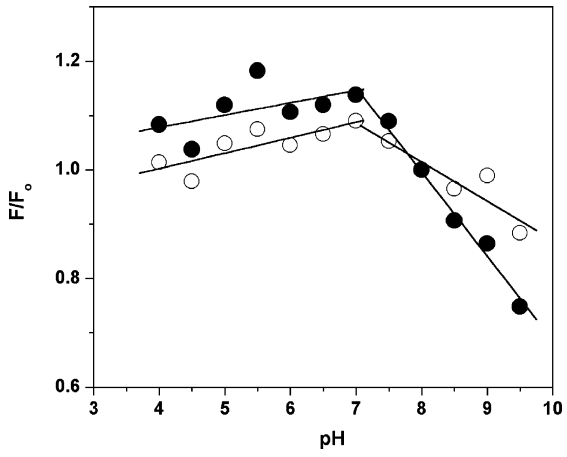

FIGURE 6: Effect of pH on the steady-state intrinsic fluorescence of ostreolysin (5.13 μg/mL) in the absence (○) or presence (●) of SEL SUV at a lipid:protein ratio of 3.25 (w/w). Data are normalized to the fluorescence intensity of the protein at pH 8.0 (F_o). Excitation was at 295 nm, and emission was at 339 nm.

of secondary structure but a low content of tertiary structure (*32*).

pH-induced conformational changes of ostreolysin were also monitored using UV absorption spectroscopy (not shown). The resulting titration curve was qualitatively in good agreement with the CD and fluorescence data.

ANS Binding to Ostreolysin. To provide additional evidence for the molten globule-like state of ostreolysin, we employed the external fluorescent probe ANS (*31*, *32*). The fluorescence of ANS was quenched by the bulk polar solvent. However, if bound to protein hydrophobic surfaces, it fluoresces as noticed with acid-denatured ostreolysin (data not shown). Both the increased ANS fluorescence intensity and the blue shift from 520 to 490 nm indicated that ostreolysin adopted a conformational state with hydrophobic sites accessible to the dye. The molten globule-like conformation appeared to be most populated at pH ~2.5 (data not shown). The absence of ANS fluorescence during base-induced denaturation of ostreolysin (data not shown) suggests the formation of a more expanded conformational state (e.g., pre-molten globule-like state). In contrast, some proteins form the molten globule-like state at high pH, but only in the presence of high salt concentrations (*33*−*35*).

Fluorescence Titration of Lipid-Bound Ostreolysin. Binding of ostreolysin to SEL LUV resulted in a slight increase in the intensity of tryptophan fluorescence (~10−15%) (*12*), but not to Chol/SM (1:1) LUV (unpublished results). Thus, it appears that ostreolysin tryptophan residues are neither involved in binding to the lipid bilayer nor translocated into the membrane hydrophobic core. This enabled us to compare the tryptophan fluorescence of free and lipid-bound ostreolysin without interference of a lipid-induced increase in intrinsic tryptophan fluorescence as reported for some pore-forming proteins (*36*−*39*). Figure 6 shows that certain tryptophan residues, in either free or bound protein, became more solvent-exposed at pH 7−8. However, the degree of fluorescence quenching with an increase in pH was enhanced in the lipid-bound ostreolysin. This suggests that when ostreolysin is lipid-bound its conformation is changed more extensively relative to the free form since some tryptophan residues are more accessible to the bulk polar solvent.

Heat-Induced Conformational Transitions of Ostreolysin. The melting profile of ostreolysin was followed at 245 nm, the wavelength at which the difference in absorbance between the native and denatured states of the protein was maximal (data not shown). Assuming that the heat-induced conformational transition of ostreolysin is a reversible two-state transition, the van't Hoff enthalpy of denaturation, $\Delta H°_{vH}$, was determined as a function of pH (Table 1). The thermal stability was highest at pH 8.0, with a denaturation enthalpy of 584 kJ/mol, and lower at pH 6.0 and 9.0, where T_d differed by approximately 1 °C (Table 1). In the pH range from 6 to 11, the heat-induced transition was cooperative, suggesting that, in this range, the protein retains its globular structure. At pH 3, however, a monotonic increase in absorbance with temperature was observed, suggesting that the transition was noncooperative (data not shown). At pH 7.0, the denaturation profile of ostreolysin monitored at 245 nm exhibited a biphasic transition (data not shown), the first at 47.2 °C and the second at 54.6 °C.

The values of $\Delta H°_{vH}$ obtained in the ostreolysin solution at different pHs (Table 1) increase linearly with the temperature of half-transition, T_d, and the slope of $\delta(\Delta H°_{vH})/\delta T_d$ coincides quantitatively with the apparent standard heat capacity difference between the denatured and native state of the protein, $\Delta C_p°$ (*40*). The value of $\Delta C_p°$ was 12.0 ± 0.9 kJ mol^{-1} K^{-1}. Experimental determination of $\Delta H°_{vH}$, T_d, and $\Delta C_p°$ allows us to calculate the temperature dependence of the denaturation enthalpy, $\Delta H°_d(T)$, entropy, $\Delta S°_d(T)$, and Gibbs free energy, $\Delta G°_d(T)$. Assuming that in the temperature range between 20 and 80 °C, $\Delta C_p°$ is constant and independent of the media in which ostreolysin conformational transitions take place and provided that an aggregation of the unfolded protein molecules at higher temperatures does not occur, one obtains (*40*, *41*)

$$\Delta H°_d(T) = \Delta H°_{vH} - \int_T^{T_d} \Delta C_p° \, dT = \Delta H°_{vH} - \Delta C_p°(T_d - T) \quad (2)$$

$$\Delta S°_d(T) = \frac{\Delta H°_{vH}}{T_d} - \int_T^{T_d} \frac{\Delta C_p°}{T} \, dT = \frac{\Delta H°_{vH}}{T_d} - \Delta C_p° \ln\left(\frac{T_d}{T}\right) \quad (3)$$

$$\Delta G°_d(T) = \Delta H°_d(T) - T\Delta S°_d(T) \quad (4)$$

The values of $\Delta H°_d(T)$, $\Delta S°_d(T)$, and $\Delta G°_d(T)$ calculated at 25 °C for ostreolysin at different pH values are listed in Table 2. They show that ostreolysin has a $\Delta G°_d(T)$ value of ~30 kJ/mol in the pH range from 6 to 9 and the highest stability at pH 8. At pH 11, the value of $\Delta G°_d(T)$ is 4-fold lower than that at pH 8.0. At pH 7.0, the transition of ostreolysin was biphasic (data not shown), and the thermodynamic quantities cannot be calculated on the basis of the model we applied. The inspection of Table 2 reveals that the enthalpic contribution that favors the stability of the native form increases with pH (from pH 8 to 11), like the entropic contribution that favors the denatured form. Our thermodynamic data (Table 2) reveal that correlation between $\Delta H°_d(T)$ and $\Delta G°_d(T)$ is very poor, indicating no mutual dependence between the two variables (*42*). The enthalpy−

Table 1: Denaturation Temperature (T_d) and Thermodynamic Characteristics of the Thermally Induced Transitions of Ostreolysin at Different pH Values Obtained from UV Absorbance Melting Experiments[a]

pH	T_d (°C)	ΔT (°C)	$\Delta H°_{vH}$ (kJ/mol)
11.0	34.6 ± 0.5	8.0	393
10.0	39.4 ± 0.5	7.6	426
9.0	47.2 ± 0.5	6.3	543
8.0	51.2 ± 0.5	6.0	584
7.0			
first transition	47.2 ± 0.5	–	–
second transition	54.6 ± 0.5	–	–
6.0	48.6 ± 0.5	6.3	546

[a] UV absorbance was monitored at 245 nm. T_d is the temperature midpoint of denaturation. ΔT is the width of the transition. $\Delta H°_{vH}$ is the van't Hoff enthalpy of denaturation assuming a reversible two-state transition. The estimated error of our measurements is 10%.

Table 2: Thermodynamic Profile of Ostreolysin Stability at 25 °C at Different pH Values Calculated from UV Melting Results by Using eqs 2−4[a]

pH	$\Delta H°_d$[b] (kJ/mol)	$\Delta S°_d$[b] (kJ mol^{-1} K^{-1})	$\Delta G°_d$[b] (kJ/mol)
11.0	278	0.90	9.7
10.0	253	0.80	14.5
9.0	277	0.83	29.5
8.0	270	0.79	37.4
7.0	–	–	–
6.0	263	0.78	30.4

[a] The value of the difference in standard molar heat capacities between the native and denatured state, $\Delta C_p°$, used in all calculations was 12.0 kJ mol^{-1} K^{-1}. [b] The relative error is estimated to be ±10−20%.

entropy compensation is more pronounced at higher pH values, resulting in a smaller net free energy change. This behavior was proposed to result from water molecule reorganization, which contributed significantly to the enthalpy and entropy changes (*42*). The thermodynamic profile of ostreolysin reported at 25 °C (Table 2) is based on the model-dependent determination of $\Delta H°_{vH}$ at T_d from UV melting experiments. To gain insight into the mechanism of ostreolysin unfolding, some additional experiments, by using differential scanning calorimetry (DSC) and applying model-independent determination of $\Delta H°_d$, are required. Nevertheless, the thermodynamic profile obtained from the UV absorbance melting experiments of ostreolysin supports the observations from CD and fluorescence measurements (Figure 5A,B) and indicates that ostreolysin loses its globular structure at pH >11 and <3.5.

Heat-Induced Denaturation of Ostreolysin at pH 7 and 8 Studied by CD Spectroscopy. To characterize the biphasic behavior of ostreolysin unfolding at pH 7 (data not shown) in more detail, we recorded far- and near-UV CD spectra in the range from 20 to 95 °C at pH 8.0 (Figure 7A) and 7.0 (Figure 7B). The melting profiles differed at these two pHs. The values for T_d, determined from the molar ellipticity at pH 8.0 at 293 and 210 nm (Figure 7A, inset), were very similar (50 ± 1 °C), while at pH 7.0, they were 50 ± 1 and 54 ± 1 °C, respectively (Figure 7B, inset). Moreover, at pH 7, secondary structure appeared to be more thermally stable than at pH 8 (note the broader interval of induced α-helical structure, insets of panels A and B of Figure 7). For comparison, the amount of α-helical structure at 80 °C is ∼20% at pH 7 and ∼5% at pH 8. These data suggest that

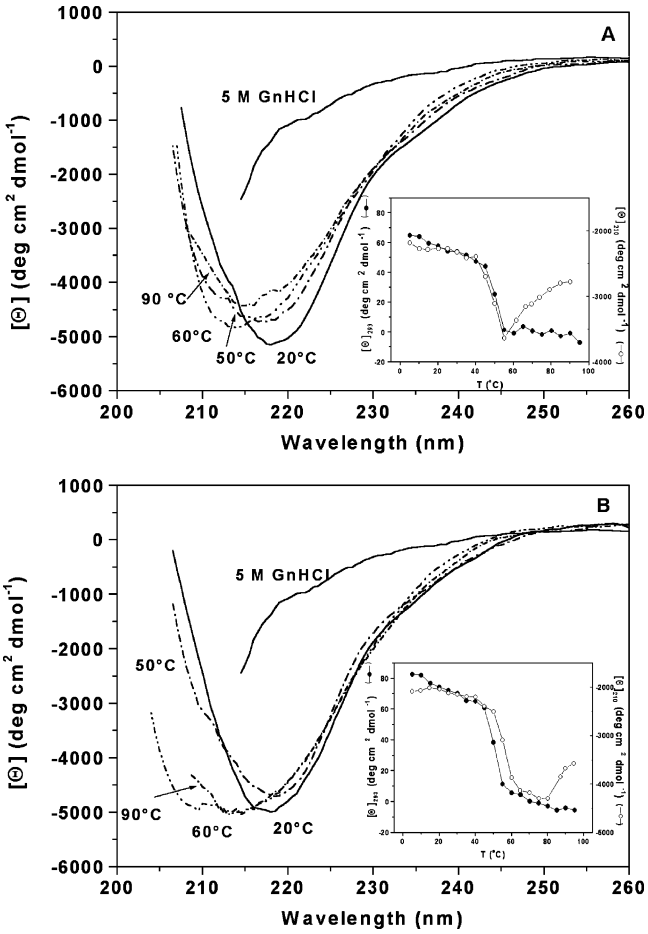

FIGURE 7: Far- and near-UV CD spectra of 66.7 μM ostreolysin at pH 8 (A) and 7.0 (B) at selected representative temperatures, and in the presence of 5 M GnHCl. Insets show changes in the molar ellipticity of ostreolysin at 293 (●) and 210 nm (○) as a function of temperature. The buffer solution was 10 mM HEPES.

ostreolysin at pH 7 in the temperature interval from 65 to 80 °C exists in a high-temperature intermediate state characterized by a lack of tertiary structure and induced, non-native α-helical structure. A similar high-temperature intermediate state with a lack of tertiary structure and induced non-native α-helical secondary structure was observed for cytolytic pore-forming protein equinatoxin II in the acidic pH range (*43*).

DISCUSSION

Our main objective was to correlate conformational states of ostreolysin with its function of binding to lipids and pore formation. For a number of pore-forming proteins, it has been reported that their action is dependent on their specific conformational states. The protein unfolding, leading to lipid insertion and/or to induction of an oligomerization-competent form, could be provoked by low pH, chemical denaturants, detergents, electrostatic and/or hydrophobic interaction of the protein with lipid membrane surface, limited proteolysis, or binding to a specific membrane receptor (see, for example, refs *37* and *44*−*50*). Here, we demonstrate that (i) ostreolysin, a small β-structured protein, binds to membrane lipids with a pH optimum of ∼6−7 in a nativelike conformation [$\Delta G°_d$(25 °C) = 30.4 kJ/mol], (ii) its pore forming activity on both natural and artificial lipid membranes is maximal at pH ∼7.8−8, coinciding with a maximal conformational

stability [$\Delta G°_d$(25 °C) = 37.4 kJ/mol], and (iii) the acid-induced molten globule-like conformation is important for neither lipid binding nor pore formation.

Interpretation of denaturation−function studies relies on knowledge of the protein conformational structure. In general, a protein multidomain structure, known for a number of bacterial pore-forming toxins (see, for example, ref *16*), may result in a complex unfolding pathway due to individual domain behavior, as found for *Bacillus thuringiensis* Cry1Ab toxin (*51*). Our interpretation of the conformational changes of ostreolysin and their relevance for the activity is based on the assumption that it is a single-domain protein. This is consistent with the rather low molecular weight (137 amino acid residues) [more than 80% of proteins with fewer than 220 amino acid residues have one domain (*52*, *53*)] and with our 3D-PSSM prediction for ostreolysin (see Results).

Another issue to be clarified was the potential role of the two cysteine residues in stabilizing the protein conformation by formation of a disulfide bond, with possible consequences for the protein function. In SDS−PAGE (in the absence of reducing agents) of ostreolysin, two closely positioned bands have been regularly observed (1, 12, and 13, and Figure 3 herein), despite a single species being confirmed by ESI-MS (*13*) and N-terminal microsequencing (unpublished data). It has been suggested that two conformational isoforms are ascribed to a partial intramolecular S−S bonding of the cysteines (*1*). The use of DTT and oxidized glutathione strongly suggests that there is no intramolecular disulfide bonding, or if there is some, it is far from complete. It appears rather that cysteine(s) should be free in the active protein as proven previously by the use of thiol-reactive agents (*1*, *21*), and that spontaneous intramolecular disulfide formation could not be affecting the observed changes in protein conformation.

The combined unfolding results suggest that ostreolysin at 25 °C can take on several spectroscopically distinct states due to deprotonation equilibria of ionic amino acid side chains (Figure 5A,B), but only four thermodynamically stable conformational states as summarized by the scheme

$$D_a \leftrightarrow MG \leftarrow N \rightarrow D_b$$

where D_a denotes the acid-denatured state, MG the molten globule, N the native state, and D_b the base-denatured state. The characteristics of acid unfolding of ostreolysin are similar to those found for type I proteins (*54*), with the appearance of a molten globule-like state at pH ∼2−3. The acid-induced molten globule state of ostreolysin is characterized by a complete absence of tertiary structure, well-pronounced non-native secondary structure, and high affinity for ANS (*55*). The pH and thermal denaturation data reveal that ostreolysin is in the most thermodynamically stable, native conformation N, near pH ∼8. Isoelectric precipitation observed below pH 6 precluded recording of reliable reporting spectra and conformational characterization at low pH values; however, we found ostreolysin bound (Figure 3) and active on lipid vesicles at higher ostreolysin concentrations at pH 4−6 (unpublished). At pH ∼12, we suspect that ostreolysin might adopt a conformational state exhibiting some similarities with the acid-induced molten globule state, but it is more expanded as based on the estimated amount of secondary structure and does not bind the ANS. At pH >12, ostreolysin adopted a base-denatured conformation, which is characterized by the loss of tertiary structure and residual of secondary structures, which corresponded to a complete loss of the protein function.

The pH optima of ostreolysin pore forming activity, measured as the rate of calcein release from vesicles and hemolysis (Figure 2), do not overlap with the pH for maximum binding to lipid vesicles (Figure 3). The base-shifted pH optimum of calcein release from SEL LUV as compared to hemolysis could be ascribed to differences in the membrane composition, with more negative charges on the erythrocytes due to the presence of sialylated proteins such as glycophorin. In contrast to several pore-forming proteins, binding of ostreolysin to lipid membranes does not involve either an acid- or a base-induced molten globule-like state, but a thermodynamically stable nativelike conformation. This suggests that binding to the lipid bilayer should evoke further conformational transition(s) necessary for insertion and pore formation. In fact, this is supported by the results of tryptophan fluorescence pH titration of free and lipid-bound ostreolysin (Figure 6), which shows some indolyl residues to be more exposed if ostreolysin is combined with lipids. Moreover, the similar pattern of the titration curves, with and without lipid, implies a very similar pattern of subtle unfolding of the protein, which is, however, more extensive on the lipid membrane. This lipid-enhanced transition may be related to the spectroscopically observed local changes between pH 7 and 8. Additionally, at pH 7, ostreolysin exhibits a biphasical thermal transition as can be observed from UV (data not shown) and CD melting profiles (Figure 7B). This may be related to deprotonation of two histidine residues governed by a pK_a ranging from 6.7 to 7.4 as expected in proteins, and/or deprotonation of cysteines with a pK_a of ∼8. However, further experiments are required to clarify if and how these conformational changes, and their resulting conformational states, relate to the activity.

In conclusion, our study suggests that ostreolysin, and probably other proteins of the aegerolysin family (including those from the pathogenic moulds *A. fumigatus*, *Pa. brasiliensis*, and *C. immitis*), binds to the lipid membrane surface in a compact, nativelike conformation. Further conformational transition(s), necessary for translocation of a particular part of the polypeptide chain, are subtle, preserving very likely the β-fold structure intact. In general, this mechanism is similar to the one observed for another family of small, single-domain, pore-forming proteins, the actinoporins from sea anemones. These pore-forming toxins, with dominant β-structure, perforate the lipid bilayer with an N-terminal amphiphilic α-helix. This is the only part of the polypeptide chain dislocated from a stable β-sandwich structure, which resides meanwhile on the membrane surface (*22*, *56*−*58*). Other similarities to actinoporins are the appearance of a molten globule-like state at low pH and the optimum of pore forming activity at pH ∼8 (*59*, *60*). We suggest that, in addition to the class of pore-forming proteins which act through a "molten globule mechanism", introduced by van der Goot et al. (*61*), there is a separate group, exemplified by equinatoxin and ostreolysin. These proteins differ in being characterized structurally by a dominant β-structure scaffold that keeps a constant global domain tertiary structure, while the polypeptide elements needed for membrane penetration

are provided by minor local conformational changes. This mechanism, using a more or less compact scaffold, may play a role even in multidomain proteins. In such a case, however, a coordinated interplay of changes in other domains is expected, as shown for bacterial perfringolysin O (*62*).

ACKNOWLEDGMENT

We thank Dr. Eva Žerovnik from the Institute of Jožef Stefan (Ljubljana, Slovenia) for her help with CD measurements and Mrs. Irena Pavešiæ from the Department of Biology, Biotechnical Faculty, University of Ljubljana, for purification of ostreolysin. We are especially grateful to Dr. Roger Pain for critical reading of the manuscript and many helpful suggestions.

REFERENCES

1. Berne, S., Križaj, I., Pohleven, F., Turk, T., Maček, P., and Sepčić, K. (2002) *Pleurotus* and *Agrocybe* hemolysins, new proteins hypothetically involved in fungal fruiting, *Biochim. Biophys. Acta 1570*, 153−159.
2. Fernandez-Espinar, M.-T., and Labarère, J. (1997) Cloning and sequencing of the Aa-Pri1 gene specifically expressed during fruiting initiation in the edible mushroom *Agrocybe aegerita*, and analysis of the predicted amino acid sequence, *Curr. Genet. 32*, 420−424.
3. Ebina, K., Sakagami, H., Yokota, K., and Kondo, H. (1994) Cloning and nucleotide sequence of cDNA encoding Asp-hemolysin from *Aspergillus fumigatus*, *Biochim. Biophys. Acta 1219*, 148−150.
4. Tomita, T., Noguchi, K., Mimuro, H., Ukaji, F., Ito, K., Sugawara-Tomita, N., and Hashimoto, Y. (2004) Pleurotolysin, a novel sphingomyelin-specific two-component cytolysin from the edible mushroom *Pleurotus ostreatus*, assembles into a transmembrane pore complex, *J. Biol. Chem. 279*, 26975−26982.
5. Sakurai, N., Kaneko, J., Kamio, Y., and Tomita, T. (2004) Cloning, expression, and pore-forming properties of mature and precursor forms of pleurotolysin, a sphingomyelin-specific two-component cytolysin from the edible mushroom *Pleurotus ostreatus*, *Biochim. Biophys. Acta 1679*, 65−73.
6. Barloy, F., Lecadet, M. M., and Delécluse, A. (1998) Cloning and sequencing of three new putative toxin genes from *Clostridium bifermentans* CH18, *Gene 211*, 293−299.
7. Stover, C. K., Pham, X. Q., Erwin, A. L., Mizoguchi, S. D., Warrener, P., Hickey, M. J., Brinkman, F. S. L., Hufnagle, W. O., Kowalik, D. J., Lagrou, M., Garber, R. L., Goltry, L., Tolentino, E., Westbrock-Wadman, S., Yuan, Y., Brody, L. L., Coulter, S. N., Folger, K. R., Kas, A., Larbig, K., Lim, R., Smith, K., Spencer, D., Wong, G. K.-S., Wu, Z., Paulsen, I. T., Reizer, J., Saier, M. H., Hancock, R. E. W., Lory, S., and Olson, M. V. (2000) Complete genome sequence of *Pseudomonas aeruginosa* PA01, an opportunistic pathogen, *Nature 406*, 959−964.
8. Galagan, J. E., Calvo, S. E., Borkovich, K. A., Selker, E. U., Read, N. D., Jaffe, D., FitzHugh, W., Ma, L. J., Smirnov, S., Purcell, S., Rehman, B., Elkins, T., Engels, R., Wang, S., Nielsen, C. B., Butler, J., Endrizzi, M., Qui, D., Ianakiev, P., Bell-Pedersen, D., Nelson, M. A., Werner-Washburne, M., Selitrennikoff, C. P., Kinsey, J. A., Braun, E. L., Zelter, A., Schulte, U., Kothe, G. O., Jedd, G., Mewes, W., Staben, C., Marcotte, E., Greenberg, D., Roy, A., Foley, K., Naylor, J., Stange-Thomann, N., Barrett, R., Gnerre, S., Kamal, M., Kamvysselis, M., Mauceli, E., Bielke, C., Rudd, S., Frishman, D., Krystofova, S., Rasmussen, C., Metzenberg, R. L., Perkins, D. D., Kroken, S., Cogoni, C., Macino, G., Catcheside, D., Li, W., Pratt, R. J., Osmani, S. A., DeSouza, C. P., Glass, L., Orbach, M. J., Berglund, J. A., Voelker, R., Yarden, O., Plamann, M., Seiler, S., Dunlap, J., Radford, A., Aramayo, R., Natvig, D. O., Alex, L. A., Mannhaupt, G., Ebbole, D. J., Freitag, M., Paulsen, I., Sachs, M. S., Lander, E. S., Nusbaum, C., and Birren, B. (2003) The genome sequence of the filamentous fungus *Neurospora crassa*, *Nature 422*, 859−868.
9. Vidic, I., Berne, S., Drobne, D., Maček, P., Frangež, R., Turk, T., Štrus, J., and Sepčić, K. (2005) Temporal and spatial expression of ostreolysin during development of the oyster mushroom (*Pleurotus ostreatus*), *Mycol. Res. 109*, 377−382.
10. Kudo, Y., Ootani, T., Kumagai, T., Fukuchi, Y., and Ebina, K. (2002) A novel oxidized low-density lipoprotein binding protein, Asp-hemolysin, recognizes lysophosphatidylcholine, *Biol. Pharm. Bull. 25*, 787−790.
11. Kumagai, T., Kudo, Y., Fukuchi, Y., Ebina, K., and Yokota, K. (2002) Expression of a synthetic gene encoding the Asp-hemolysin from *Aspergillus fumigatus* in *Escherichia coli*, *Pharm. Bull. 25*, 115−117.
12. Sepčić, K., Berne, S., Potrich, C., Turk, T., Maček, P., and Menestrina, G. (2003) Interaction of ostreolysin, a cytolytic protein from the edible mushroom *Pleurotus ostreatus*, with lipid membranes and modulation by lysophospholipids, *Eur. J. Biochem. 270*, 1199−1210.
13. Sepčić, K., Berne, S., Rebolj, K., Batista, U., Plemenitaš, A., Šentjurc, M., and Maček, P. (2004) Ostreolysin, a pore-forming protein from the oyster mushroom, interacts specifically with membrane cholesterol-rich lipid domains, *FEBS Lett. 575*, 81−85.
14. Prakash, S., and Matouschek, A. (2004) Protein unfolding in the cell, *Trends Biochem. Sci. 29*, 593−600.
15. Gouaux, E. (1997) Channel-forming toxins: Tales of transformations, *Curr. Opin. Struct. Biol. 7*, 566−573.
16. Parker, M. W., and Feil, S. C. (2005) Pore-forming protein toxins: From structure to function, *Prog. Biophys. Mol. Biol. 88*, 91−142.
17. *Pharmacia PhastSystem Users Manual* (1987) Pharmacia LKB Biotechnology, Uppsala, Sweden.
18. Maček, P., and Lebez, D. (1981) Kinetics of hemolysis induced by equinatoxin, a cytolytic toxin from the sea anemone *Actinia equina*. Effects of some ions and pH, *Toxicon 19*, 233−244.
19. Menestrina, G. (1988) *Escherichia coli* hemolysin permeabilises small unilamellar vesicles loaded with calcein by a single hit mechanism, *FEBS Lett. 232*, 217−220
20. Provencher, S. W., and Glöckner, J. (1981) Estimation of globular protein secondary structure from circular dichroism, *Biochemistry 20*, 33−37.
21. Kamaguchi, A., Yokota, K., and Sakaguchi, O. (1979) Investigation of the hemolytic site of Asp-hemolysin, *Jpn. J. Med. Sci. Biol. 32*, 118−121.
22. Hong, Q., Gutiérrez-Aguirre, I., Barliè, A., Malovrh, P., Kristan, K., Podlesek, Z., Maček, P., Turk, D., González-Mañas, J. H., Lakey, J. H., and Anderluh, G. (2002) Two-step membrane binding by equinatoxin II, a pore-forming toxin from the sea anemone, involves an exposed aromatic cluster and a flexible helix, *J. Biol. Chem. 277*, 41916−41924.
23. Ramachandran, R., Heuck, A. P., Tweten, R. K., and Johnson, A. E. (2002) Structural insights into the membrane-anchoring mechanism of a cholesterol-dependent cytolysin, *Nat. Struct. Biol. 9*, 823−827.
24. Palmer, M. (2004) Cholesterol and the activity of bacterial toxins, *FEMS Microbiol. Lett. 238*, 281−289.
25. Rost, B., and Sander, C. (1994) Combining evolutionary information and neural networks to predict protein secondary structure, *Proteins 19*, 55−72.
26. Combet, C., Blanchet, C., Geourjon, C., and Deléage, G. (2000) NPS@: Network Protein Sequence Analysis, *Trends Biochem. Sci. 25*, 147−150.
27. Kelley, L. A., MacCallum, R. M., and Sternberg, M. J. E. (2000) Enhanced genome annotation using structural profiles in the program 3D-PSSM, *J. Mol. Biol. 299*, 499−520.
28. Sreerama, N., and Woody, R. W. (2000) Circular dichroism of peptides and proteins, in *Circular Dichroism: Principles and Applications*, 2nd ed., pp 601−620, John Wiley & Sons, New York.
29. Barker, R. (1971) *Organic Chemistry of Biological Compounds*, Prentice-Hall, Englewood Cliffs, NJ.
30. Gordon, D. J., and Holzwarth, G. (1971) Artifacts in measured optical activity of membrane suspensions, *Arch. Biochem. Biophys. 142*, 481−488.
31. Lakowicz, J. R. (1999) *Principles of fluorescence spectroscopy*, 2nd ed., pp 445−486, Kluwer Academic/Plenum Publishers, New York.
32. Ptitsyn, O. B. (1995) Molten globule and protein folding, *Adv. Protein Chem. 47*, 83−229.
33. Goto, Y., and Fink, A. L. (1989) Conformational states of β-lactamase: Molten-globule states at acidic and alkaline pH with high salt, *Biochemistry 28*, 945−952.

34. Edwin, F., and Jagannadham, M. V. (2000) Salt-induced folding of a rabbit muscle pyruvate kinase intermediate at alkaline pH, *J. Protein Chem. 19*, 361−371.
35. Ashraf, M. T., and Khan, R. H. (2005) Effect of metal ions and EGTA on the optical properties of concanavalin A at alkaline pH, *Protein Pept. Lett. 12*, 203−206.
36. Maček, P., Zecchini, M., Pederzolli, C., Dalla Sera, M., and Menestrina, G. (1995) Intrinsic tryptophan fluorescence of equinatoxin II, a pore-forming polypeptide from the sea anemone *Actinia equina* L., monitors its interaction with lipid membrane, *Eur. J. Biochem. 234*, 329−335.
37. Nakamura, M., Sekino, N., Iwamoto, M., and Ohno-Iwashita, Y. (1995) Interaction of θ-toxin (perfringolysin O), a cholesterol-binding cytolysin, with liposomal membranes: Change in the aromatic side chains upon binding and insertion, *Biochemistry 34*, 6513−6520.
38. Ostolaza, H., and Goñi, F. M. (1995) Interaction of the bacterial protein toxin α-haemolysin with model membranes: Protein binding does not always lead to lytic activity, *FEBS Lett. 371*, 303−306.
39. Nollmann, M., Gilbert, R., Mitchell, T., Sferrazza, M., and Byron, O. (2004) The role of cholesterol in the activity of pneumolysin, a bacterial protein toxin, *Biophys. J. 86*, 3141−3151.
40. Privalov, P. L., and Khechinashvili, N. N. (1974) Thermodynamic approach to problem of stabilization of globular protein structure: Calorimetric study, *J. Mol. Biol. 86*, 665−684.
41. Becktel, W. J., and Schellman, J. A. (1987) Protein stability curves, *Biopolymers 26*, 1859−1877.
42. Liu, L., Yang, C., and Guo, Q.-X. (2000) A study on the enthalpy−entropy compensation in protein unfolding, *Biophys. Chem. 84*, 239−251.
43. Poklar, N., Lah, J., Salobir, M., Maček, P., and Vesnaver, G. (1997) pH and temperature-induced molten globule-like denatured states of equinatoxin II: A study by UV-melting, DSC, far- and near-UV CD spectroscopy, and ANS fluorescence, *Biochemistry 36*, 14345−14352.
44. Merrill, A. R., Cohen, F. S., and Cramer, W. A. (1990) On the nature of the structural change of the colicin E1 channel peptide necessary for its translocation, *Biochemistry 29*, 5829−5836.
45. Vécsey-Semjén, B., Möllby, R., and van der Goot, F. G. (1996) Partial C-terminal unfolding is required for channel formation by staphylococcal α-toxin, *J. Biol. Chem. 271*, 8655−8660.
46. Bortoleto, R. K., and Ward, R. J. (1999) A stability transition at mildly acidic pH in the α-hemolysin (α-toxin) from *Staphylococcus aureus*, *FEBS Lett. 459*, 438−442.
47. Guihard, G., Laprade, R., and Schwartz, J. L. (2001) Unfolding of insect cell permeabilization by *Bacillus thuringiensis* Cry1C toxin, *Biochim. Biophys. Acta 1515*, 110−119.
48. Gupta, P. K., Kurupati, R. K., Chandra, H., Gaur, R., Tandon, V., Singh, Y., and Maithal, K. (2003) Acid unfolding of anthrax protective antigen, *Biochem. Biophys. Res. Commun. 311*, 229−232.
49. Krantz, B. A., Trivedi, A. D., Cunningham, K., Christensen, K. A., and Collier, R. J. (2004) Acid-induced unfolding of the amino-terminal domains of the lethal and edema factors of anthrax toxin, *J. Mol. Biol. 344*, 739−756.
50. Oh, K. J., Barbuto, S., Meyer, N., Kim, R.-S., Collier, R. J., and Korsmeyer, S. J. (2005) Conformational changes in BID, a pro-apoptotic BCL-2 family member, upon membrane binding. A site-directed spin labeling study, *J. Biol. Chem. 280*, 753−767.
51. Rausell, C., Pardo-Lopez, L., Sanchez, J., Munoz-Garay, C., Morera, C., Soberon, M., and Bravo, A. (2004) Unfolding events in the water-soluble monomeric Cry1Ab toxin during transition to oligomeric pre-pore and membrane-inserted pore channel, *J. Biol. Chem. 279*, 55168−55175.
52. Corpet, F., Servant, F., Gouzy, J., and Kahn, D. (2000) ProDom and ProDom-CG: Tools for protein domain analysis and whole genome comparisons, *Nucleic Acids Res. 28*, 267−269.
53. Marsden, R. L., McGuffin, L. J., and Jones, D. T. (2002) Rapid protein domain assignment from amino acid sequence using predicted secondary structure, *Protein Sci. 11*, 2814−2824.
54. Fink, A. L., Calciano, L. J., Goto, Y., Kurotsu, T., and Palleros, D. R. (1994) Classification of acid denaturation of proteins: Intermediates and unfolded states, *Biochemistry 33*, 12504−12511.
55. Ptitsyn, O. B. (1995) Molten globule and protein folding, *Adv. Protein Chem. 47*, 83−228.
56. Athanasiadis, A., Anderluh, G., Maček, P., and Turk, D. (2001) Crystal structure of the soluble form of equinatoxin II, a pore-forming toxin from the sea anemone *Actinia equina*, *Structure 9*, 341−346.
57. Mancheño, J. M., Martin-Benito, J., Martinez-Ripoll, M., Gavilanes, J. G., and Hermoso, J. A. (2003) Crystal and electron microscopy structures of sticholysin II actinoporin reveal insights into the mechanism of membrane pore formation, *Structure 11*, 1319−1328.
58. Kristan, K., Podlesek, Z., Hojnik, V., Gutierrez-Aguirre, I., Guncar, G., Turk, D., Gonzalez-Manas, J. M., Lakey, J. H., Maček, P., and Anderluh, G. (2004) Pore formation by equinatoxin, a eukaryotic pore-forming toxin, requires a flexible N-terminal region and a stable β-sandwich, *J. Biol. Chem. 279*, 46509−46517.
59. Poklar, N., Volker, J., Anderluh, G., Maček, P., and Chalikian, T. V. (2001) Acid- and base-induced conformational transitions of equinatoxin II, *Biophys. Chem. 90*, 103−121.
60. Poklar Ulrih, N., Anderluh, G., Maček, P., and Chalikian, T. V. (2004) Salt-induced oligomerization of partially folded intermediates of equinatoxin II, *Biochemistry 43*, 9536−9545.
61. van der Goot, F. G., Gonzalez-Mañas, J. M., Lakey, J. H., and Pattus, F. (1991) A 'molten-globule' membrane-insertion intermediate of the pore-forming domain of colicin A, *Nature 354*, 408−410.
62. Czajkowsky, D. M., Hotze, E. M., Shao, Z., and Tweten, R. K. (2004) Vertical collapse of a cytolysin prepore moves its transmembrane β-hairpins to the membrane, *EMBO J. 23*, 3206−3215.

BI051013Y